LUT University

Polyacrylonitrile-encapsulated amorphous zirconium phosphate composite adsorbent for Co, Nd and Dy separations

Xu Junhua, Virolainen Sami, Zhang Wenzhong, Kuva Jukka, Sainio Tuomo, Koivula Risto

This is a Publisher's version version of a publication

published by Elsevier

in Chemical Engineering Journal

DOI: 10.1016/j.cej.2018.06.112

Copyright of the original publication: 2018 The Authors.

Please cite the publication as follows:

Xu, J., Virolainen, S., Zhang, W., Kuva, J., Sainio, T., Koivula, R., 2018. Polyacrylonitrile-encapsulated amorphous zirconium phosphate composite adsorbent for Co, Nd and Dy separations. Chemical Engineering Journal 351, 832–840. https://doi.org/10.1016/j.cej.2018.06.112

This is a parallel published version of an original publication. This version can differ from the original published article.

Chemical Engineering Journal 351 (2018) 832–840

Contents lists available at ScienceDirect

Chemical Engineering Journal

journal homepage: www.elsevier.com/locate/cej

Polyacrylonitrile-encapsulated amorphous zirconium phosphate composite adsorbent for Co, Nd and Dy separations

Junhua Xu[a,*], Sami Virolainen[b], Wenzhong Zhang[a], Jukka Kuva[c], Tuomo Sainio[b], Risto Koivula[a]

[a] Department of Chemistry—Radiochemistry, P.O. Box 55, FI-00014 University of Helsinki, Finland
[b] Department of Chemistry, Lappeenranta University of Technology, FI-53850 Lappeenranta, Finland
[c] Geological Survey of Finland GTK, P.O. Box 96, FI-02150 Espoo, Finland

HIGHLIGHTS

- The am-ZrP evenly distributed in porous am-ZrP/PAN Beads.
- The uptake enhanced and induced from DMF intercalation.
- The real-life separation has been studied from the chemical engineering perspective.
- A gradient elution based process proposal has been constructed.
- Purity in collect fractions relative to the feed significantly improved.

GRAPHICAL ABSTRACT

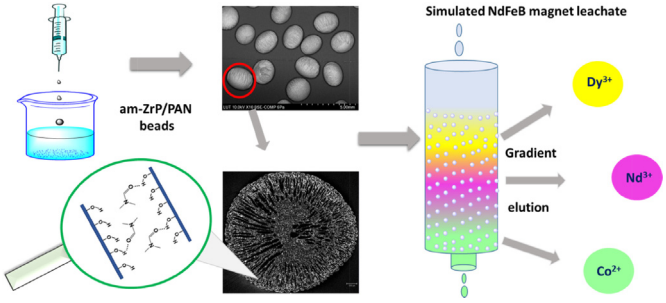

ARTICLE INFO

Keywords:
Zirconium phosphate
NdFeB magnet
Ion exchange
DMF intercalation
Rare earth separation
Gradient elution

ABSTRACT

Recycled Nd and Dy from the end-of-life NdFeB permanent magnet is an important supplement for the increasing demand of rare-earth elements. Thus, there is an urgent need to develop an environmentally friendly recycling method. Amorphous zirconium phosphate exhibits selective separation properties towards the ternary Co-Nd-Dy system, however, its powdery form limits development of scaled-up applications. We present an efficient amorphous ZrP/Polyacrylonitrile (am-ZrP/PAN) composite ion exchanger for uptake and separation of Nd, Dy and Co. The am-ZrP/PAN composite was synthesized and its structural, morphologic and acidic properties were investigated by various methods. X-ray tomography revealed rather evenly distributed am-ZrP in the PAN polymer matrix. The selectivity and ion-exchange kinetics of the am-ZrP/PAN composite were determined in relation to the individual elements. Due to dimethylformide (DMF) intercalation into the interlayer of ZrP, the uptake of Co, Nd and Dy increased 50% compared with that of the pristine am-ZrP. Column separation of Co, Nd and Dy from the Co-Nd-Dy ternary system was assessed by varying the feed concentration, loading degree, temperature, running speed and elution agent (HNO_3) concentration. Finally, gradient elution was employed for Co, Nd and Dy separation from a simulated ternary leachate. Fractions with 87.9% pure Co, 96.4% pure Nd and 40% pure Dy were collected through a single-column operation.

1. Introduction

The need for rare-earth elements (REEs) has increased due to growing demand for permanent magnets (NdFeB) in applications such as industrial motors, wind turbines, consumer electronics and electric vehicles [1]. A NdFeB magnet typically contains approximately 31–32 wt% of REEs such as Nd, Pr, Dy, Tb and Gd [2]. To improve high-temperature stability and wear and corrosion resistance of the magnet,

* Corresponding author.
E-mail address: junhua.xu@helsinki.fi (J. Xu).

https://doi.org/10.1016/j.cej.2018.06.112
Received 29 March 2018; Received in revised form 8 June 2018; Accepted 18 June 2018
Available online 19 June 2018
1385-8947/ © 2018 The Authors. Published by Elsevier B.V. This is an open access article under the CC BY license (http://creativecommons.org/licenses/BY/4.0/).

Co is often added with a comparable content of Dy [3,4]. It is estimated that over the next 25 years the demand for Nd and Dy will increase by 700% and 2600%, respectively [5]. As reported by the European Commission in 2018, REEs and Co were evaluated as critical raw materials due to economic importance and supply risk [6]. To some extent, recycled Nd and Dy as well as Co from NdFeB magnets will play significant roles in the future supply chain of critical raw materials such as REEs and Co [7,8]. We therefore sought to develop an environmentally friendly method to recycle Co, Nd and Dy from end-of-life NdFeB permanent magnets.

In commercial separations, REEs are extracted from ores using mineral acids and then separated by solvent extraction (SX), in which REEs are transferred to an organic phase using selective extractants [9]. In most cases, organophosphorous extractants, di(2-ethylhexyl)phosphoric acid (DEHPA, D2EHPA) or its ester (EHEHPA) are used. Even though organophosphorus extractants are commercially used for metal separation, the selectivity for adjacent lanthanides not ideal. Due to the similar ionic radii and coordination properties of REEs, the separation factors for neighbouring lanthanides are in the range of 1.5–3. Hundreds of separation stages (in mixer-settlers) and complicated flowsheets with reflux are thus needed to obtain an individual REE [10,11]. The use of often toxic and volatile organic chemicals in the SX process is also further incentive to develop ecologically responsible separation techniques, such as ion exchange.

Currently, although solvent extraction is used in large-scale production of REEs, ion-exchange technology is used to produce high-purity REEs [12,13]. Inorganic ion exchangers are extensively applied for adsorption and purification due to high selectivity, stability in relatively high temperatures and resistance to ionizing radiation [14]. Our earlier studies with crystalline and amorphous zirconium phosphates (α-ZrP and am-ZrP) on uptake and elution from a ternary Co-Nd-Dy system showed promising individual recovery of the metals [15,16]. However, the powdery form of these materials led to potential operational problems, such as pressure build-up and clogging in column operations [17,18].

To overcome these problems, it is vital to increase the material's particle size. One possibility is to produce hybrid composites by embedding the inorganic particles onto porous granulated carriers [18–21]. Polyacrylonitrile (PAN) possesses excellent physicochemical characteristics such as pelletizing properties, strong adhesive forces with inorganic materials and good chemical stability [22–24]. Hence, the ion-exchange material can be effectively immobilized into spherical beads and the polymer can accommodate loadings up to 95% [25,26].

Here we report the synthesis, material and ion exchange characterization of an am-ZrP/PAN composite ion exchanger for metal separations. The efficient separation of metals from a magnet leaching solution was investigated with single-column loading elution and loading-gradient elution experiments.

2. Experimental

2.1. Chemicals

Polyacrylonitrile (PAN, average Mw 150 000), dimethylformamide (DMF, > 99.9%), Tween® 80, zirconium tetrachloride ($ZrCl_4$, > 99.5%), cobalt nitrate hexahydrate ($Co(NO_3)_2{\cdot}6H_2O$, 98%), neodymium nitrate hexahydrate ($N_3NdO_9{\cdot}6H_2O$, 99.9%), dysprosium nitrate hydrate ($DyN_3O_9{\cdot}xH_2O$, 99.9%), sulfuric acid (H_2SO_4, 95–97%), hydrochloric acid (HCl, > 37%), orthophosphoric acid (H_3PO_4, 85%) and nitric acid (HNO_3, 67–69%) were purchased from Sigma-Aldrich and used without further purification. Milli-Q water (Merck Millipore) with a resistivity of 18.2 MΩ cm (at 23 °C) was used in all experiments.

2.2. Instrumentation and analysis methods

Images of the am-ZrP/PAN beads were collected by a Hitachi Hi-Tech S-4800 field-emission scanning electron microscope (FESEM) after deposition of a 3 nm-thick layer of Pd-Au by sputtering. To investigate the size distribution, uncoated am-ZrP/PAN beads were imaged by a Hitachi SU3500 scanning electron microscope. The morphology of 199 beads were analysed from the images by Malvern Morphologi G3 software. For spatial distribution of inorganic material in inner polymer matrix, the bead was identified by X-ray tomography using a GE Phoenix v|tome|x s 240 at the Geological Survey of Finland. A 180 kV/15 W optional nanofocus tube was used with a 90-kV accelerating voltage and a 300-μA current, resulting in a 27-W tube power. The sample was imaged with an isotropic 1.33-μm resolution/voxel size. 2700 projections with an exposure time of 2 × 4000 ms were taken with a 4000-ms skip at each angle. The total acquisition time was 9 h. For structural analysis of the am-ZrP/PAN composite, X-ray powder diffraction (XRD) patterns were acquired using a Philips PW 3710 X-ray diffractometer with Cu-Kα (λ = 1.542 Å) at a potential of 40 kV and a current of 40 mA. Fourier transform infrared (FT-IR) spectra were recorded by a Perkin Elmer spectrum one FT-IR spectrometer in the range of 400–4000 cm^{-1}. Thermogravimetry (TG) was performed by a Mettler Toledo TG850 in air flow with a heating rate of 10 °C min^{-1}. For analysis of Co, Nd and Dy metal ions, a microwave plasma-atomic emission spectrometer (MPAES) Agilent 4200 was used.

2.3. Synthesis of am-ZrP/PAN

Am-ZrP material was synthesized using a precipitation method based on a previous report [1]. First, 30.7 g of $ZrCl_4$ was dissolved in 430 mL of 2 M HCl. A total of 400 mL of 1.25 M H_3PO_4 was then added. The resulting precipitate remained overnight in the mother solution. After phase separation, the precipitate was treated with 1 L of 1 M HNO_3 to ensure full conversion of materials to H-form. Finally, the am-ZrP product was washed with deionized water until pH 3 was achieved and dried in an oven at 60 °C for 48 h at normal atmosphere.

The am-ZrP/PAN composite was synthesized using a procedure described previously [17,22]. Firstly, 7.2 g of am-ZrP, 84 mL of DMF and 2 mL of Tween 80 were mixed at 60 °C for 2 h by magnetic stirring to obtain a homogeneous solution. A total of 4.8 g of PAN was then added to the solution, which was continuously stirred for another 2 h. The gelation process was conducted by dripping the mixture into deionized water through a needle (0.6 mm) to obtain the gelled composite beads. The formed beads were left to age in deionized water for 24 h and washed by 2 L of deionized water. The product was dried by lyophilization with a vacuum of 0.570 mbar at −26 °C using a freeze drier (CHRIST ALPHA 1-4 LSC).

2.4. Chemical stability of am-ZrP/PAN

The chemical stability of the am-ZrP/PAN composite bead in acid solution was tested in a pH range from 0.3 to 3. This was usually performed by adding a total of 0.1 g of am-ZrP/PAN into 10 mL of acid solution and equilibrating for 5 days in a rotary mixer at room temperature (approximately 23 °C). Concentration of metal ions in the solution was measured with MPAES.

2.5. Potentiometric titration

Potentiometric titration was conducted in a series of batch experiments where 100 mg of am-ZrP/PAN or PAN beads were placed in 19 mL of 1 M $NaNO_3$ solution and titrated with different amounts of 1 M NaOH solution (25–1050 μL) before mixing for 36 h in a rotary mixer (60 rpm) at room temperature.

2.6. Kinetic study

A total of 100 mg of am-ZrP/PAN was placed in 20 mL of 1 mM equimolar Co, Nd and Dy solutions at approximately pH 3. After pre-set

time intervals in a rotary mixer (60 rpm) at room temperature, the metal concentrations of the supernatants were measured by MPAES.

2.7. Effect of pH on metal uptake

The effect of pH on metal uptake was investigated according to the following procedure. A total of 100 mg of am-ZrP/PAN was added to 20 mL of 1 mM equimolar Co, Nd and Dy solutions at approximately pH 3 and equilibrated in a rotary mixer (60 rpm) for 12 h. The pH of the solutions was then adjusted over a pH range of 1–5 with 1 M HNO_3 or 1 M NaOH. After additional mixing for 24 h, the pH and metal concentration of the supernatants were measured.

The distribution coefficient (K_d) represents the distribution of metal ions between the solution and ion- exchange material. K_d is calculated by the following equation:

$$K_d = \frac{(C_0 - C_{eq})}{C_{eq}} \times \frac{V}{m} \quad (1)$$

where C_0 is the initial metal concentration, C_{eq} is the metal concentration at equilibrium, V is the volume of solution and m is the mass of the ion exchanger.

The separation factor (SF) can be demonstrated as the comparison of distribution coefficients between one and another. The calculated equation is the following:

$$SF = \frac{K_d^A}{K_d^B} \quad (2)$$

where K_d^A and K_d^B are the distribution coefficients of ion A and ion B, respectively.

2.8. Column loading/elution experiments

Single-column tests were performed at different temperature in a glass column with an inner diameter of 1.5 cm and a height of 20 cm. The columns were packed with 3.45 g of am-ZrP/PAN beads, resulting a bed height of 15 cm.

2.8.1. Separation of Co, Nd and Dy from dilute solution

The feed solution containing 1 mM equimolar Co-Nd-Dy mixed solution was prepared at approximately pH 1.8. The column was loaded with this feed solution (1 BV/h) and washed with 6 BV of dilute HNO_3 solution (pH 1.8) (1 BV/h) before the metals were eluted by 0.1 M HNO_3 and 0.5 M HNO_3 (0.5 BV/h).

2.8.2. Separation of Co, Nd and Dy from concentrated solution

Effects of temperature, running speed and concentration of elution solution were investigated (Table 1, experiment 1–5). A concentrated Co-Nd-Dy mixed solution (1.2 g/L total, pH 1.8) was prepared containing 10.7% of Co, 41.1% of Nd and 48.2% of Dy. Table 1 shows detailed information regarding the loading and elution processes.

Table 1
Operation conditions of column loading and elution.

Experiment	loading (h)	Elution (h)	Elution speed (mL/h)	Elution agent (HNO_3/M)	Temperature (°C)
1	0.6	6	26.4	0.2	23
2	0.6	6	26.4	0.2	50
3	0.6	6	13.2	0.2	50
4	0.6	3.2	26.4	0.2	50
5	0.6	6	26.4	0.1, 0.2, 0.5 and 1	50
6	0.1	7.3	26.4	0.1, 0.2, 0.5 and 1	50

2.8.3. Separation of Co, Nd and Dy from simulated magnet leachate

A simulated leachate (7.6 g/L total) containing 1.4% of Co, 89.3% of Nd and 9.3% of Dy was prepared according to previous reports [27,28]. Column experiments using the simulated leachate as feed solution were conducted in a continuous ion-exchange workstation. The loading and elution processes were performed and are shown in experiment 6 of Table 1.

3. Results and discussion

3.1. Morphology study on am-ZrP/PAN composite

Representative micrograph images of the am-ZrP/PAN composite are shown in Fig. 1. Particle uniformity was determined by volume and number distribution based on an analysis of 199 particles. The beads showed a more or less spherical shape with a circularity value from 0.74 to 0.98 (Fig. 1a, Table 2) and an average bead size of 2 mm based on circle equivalent (CE) measurements (Table 2). Cross-sectional images of a bead show an internal porous structure, which is a desirable feature for sorption processes (Fig. 1b and c) [20].

3.2. Spatial distribution study

The spatial distribution of the am-ZrP/PAN composite was characterized by X-ray tomography. The porous nature of the beads was confirmed and the measured porosity of the beads was approximately 40% (Fig. 2a). Spatial distributions of pores, PAN matrix and am-ZrP particles were determined by measuring the volumetric fractions slice by slice (Fig. 2b). The X-axis of the distributions is thus the distance along the Z-axis of the bead (blue arrow in Fig. 2b). Contrary to the visual observations, the distributions (Fig. 2c and d) indicate that there is more am-ZrP near the surface of the beads than in the centre. They also show a thin, practically non-porous layer of PAN on the surface of the beads; after this layer the porosity is quite evenly distributed.

3.3. Structural study

The synthetic approach (Scheme 1) for the preparation of the am-ZrP/PAN beads involved the intercalation and encapsulated process.

The XRD powder patterns of am-ZrP, am-ZrP/DMF and am-ZrP/PAN are shown in Fig. 3a. The low and broad peaks are typical for amorphous or semicrystalline am-ZrP [16,29]. The addition of DMF to the am-ZrP shifts the peak at 10.0 θ degree to 8.1, indicating expansion of the ZrP interlayer from 9 to 10.8 Å. It is suggested that DMF was intercalated into the interlayer of am-ZrP during the stirring process. Successful intercalation of DMF into the interlayer of α-ZrP and α-SnP materials and its effects has been reported (Table 3) [30,31]. The intercalated basal spacing of am-ZrP was increased by approximately 1.8 Å. In addition, the H_2O molecules (diameter 2.8 Å) in the layers were replaced by DMF; hence the total space (4.6 Å) was occupied by DMF. Due to limited space (diameter of DMF 3.5 Å < total increased space 4.6 Å < double diameter of DMF 2 * 3.5 Å), it is possible that double DMF molecules were intercalated into the layer bonded by hydrogen bonding (P)-O-H···O-CH-(N) (Scheme 1) [32].

The FTIR transmittance peaks of the am-ZrP/PAN composite were identical compositions of peaks from PAN beads and am-ZrP materials, with two major bands at 954 cm^{-1} and 1047 cm^{-1} from P—O deformation and the vibration of the orthophosphate group [33]. Small bands at 1624 cm^{-1} of the —OH group were also observed in all the three spectra [34]. Symmetric P═O bands at 730 cm^{-1} was not observed due to phosphorus exists as Zr—O—P in the amorphous ZrP network [35].

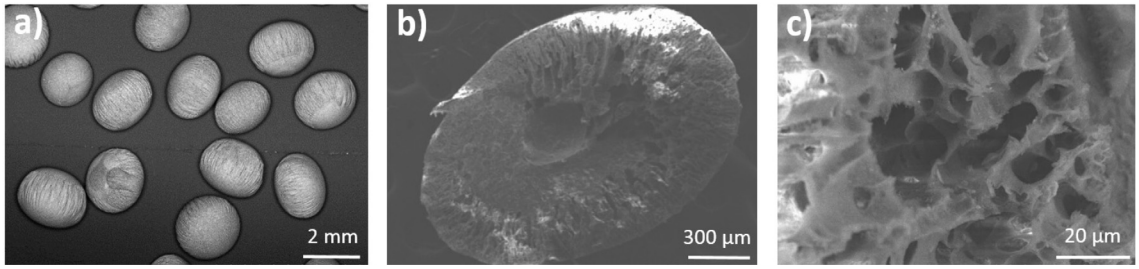

Fig. 1. a) SEM image of am-ZrP/PAN beads. b) SEM image of a cross-section of an am-ZrP/PAN bead. c) SEM image indicates the porous structure of am-ZrP/PAN.

Table 2
Particle parameters of am-ZrP/PAN as analysed by Malvern Morphologi G3 software.

	Volume distribution			Number distribution		
	Minimum	D [4,3][a]	Maximum	Minimum	Mean	Maximum
CE Diameter (µm)	1640	2035	2341	1640	2010	2341
Circularity	0.74	–	0.98	–	–	–

[a] D [4,3] is the equivalent volume mean diameter.

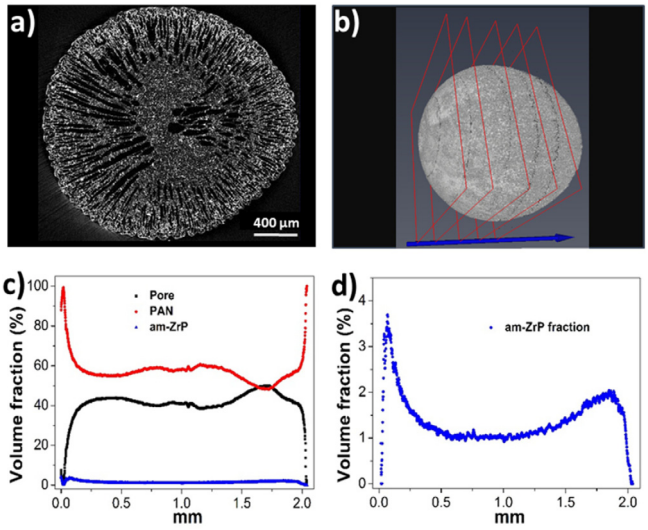

Fig. 2. a) X-ray tomography image of an am-ZrP/PAN composite sphere. b) A three-dimensional visualization of one bead and the Z-axis of the bead (blue arrow) with XY-planes used in determining the spatial distributions of components (red frames). c) Volume fraction of pores, PAN matrices and am-ZrP along the Z-axis of one bead. d) am-ZrP fraction along the Z-axis of one bead. (For interpretation of the references to colour in this figure legend, the reader is referred to the web version of this article.)

3.4. Thermal and chemical stability study

The TG curves of the PAN beads, am-ZrP and am-ZrP/PAN beads are shown in Fig. 3c. For am-ZrP/PAN beads, the 8% mass loss occurs below 300 °C and is attributed to the elimination of free water molecules. In the temperature range of 300–700 °C, weight reduction is suggested to be condensation of H_2PO_4 functional groups of am-ZrP and decomposition of PAN [36]. The composite consists of 56.7% of am-ZrP according to the thermal analysis data of PAN beads, am-ZrP and am-ZrP/PAN. The am-ZrP/PAN beads appear to be stable up to 300 °C. Chemical stability of am-ZrP/PAN was investigated by rotating the material in HNO_3 solutions of different pH (0.3, 0.9, 2 and 3). The release of Zr^{4+} was below the detection limit of MPAES (0.01 mg/L), indicating good chemical stability.

3.5. Potentiometric titration

Potentiometric titration of the PAN beads and am-ZrP/PAN beads was performed with 1 M $NaNO_3$ background solution. The conversion of am-ZrP to the Na form takes place by the following reaction:

$$POH + Na^+ \leftrightarrow PONa + H^+ \quad (3)$$

The pH of the equilibrated 1 M $NaNO_3$ solution decreased from 6.9 to 2.6 for am-ZrP/PAN. The conversion to the Na form (meq/g) can be calculated from the following:

$$q_{Na} = ([H^+]_{eq} - [H^+]_i)(V/m) \quad (4)$$

where q_{Na} is the equivalent ion-exchange capacity for Na uptake, $[H^+]_i$ is the pH value of solution before and $[H^+]_{eq}$ after equilibrating with 1 M $NaNO_3$ before NaOH addition, V is the volume of solution and m is the mass of the ion exchanger.

The q_{Na} of pure PAN beads from 1 M $NaNO_3$ was small (0.004 meq/g, Fig. 4a) and was disregarded in further calculations. The q_{Na} for am-ZrP/PAN was 0.53 meq/g as calculated by Eq. (4) (Fig. 4b). From the plateau of the titration curve, the ion-exchange capacity can be estimated; the capacity of PAN beads and am-ZrP/PAN beads is 0.46 meq/g and 4.5 meq/g, respectively (Fig. 4b) [37]. In addition, the am-ZrP content of am-ZrP/PAN beads can be calculated via the capacities of each counterpart by using a theoretical capacity of 6.97 meq/g for am-ZrP [16]. After calculation, the am-ZrP content based on ion-exchange capacity was 57.9%, which agrees well with the 56.7% content calculated from the TG results. It thus appeared that intercalation of DMF and encapsulation by PAN does not worsen the ion-exchange capacity of am-ZrP.

3.6. Adsorption kinetics

The kinetic behaviour of am-ZrP/PAN was investigated in 1 mM HNO_3 solution of Co, Nd and Dy. The uptakes for Nd and Dy equilibrated approximately 12 h (Fig. 5a), which is in line with the kinetic behaviour in the competitive adsorption onto am-ZrP in our previous study [16].

Data on adsorption kinetics (Fig. 5b) show that the uptake of metals to the am-ZrP/PAN composite is not very fast, even considering the rather large particle size of the materials (approximately 2 mm in diameter). Metal uptake increased from 50 to 70% of the equilibrium value in 30 min. The diffusion coefficients were estimated using an

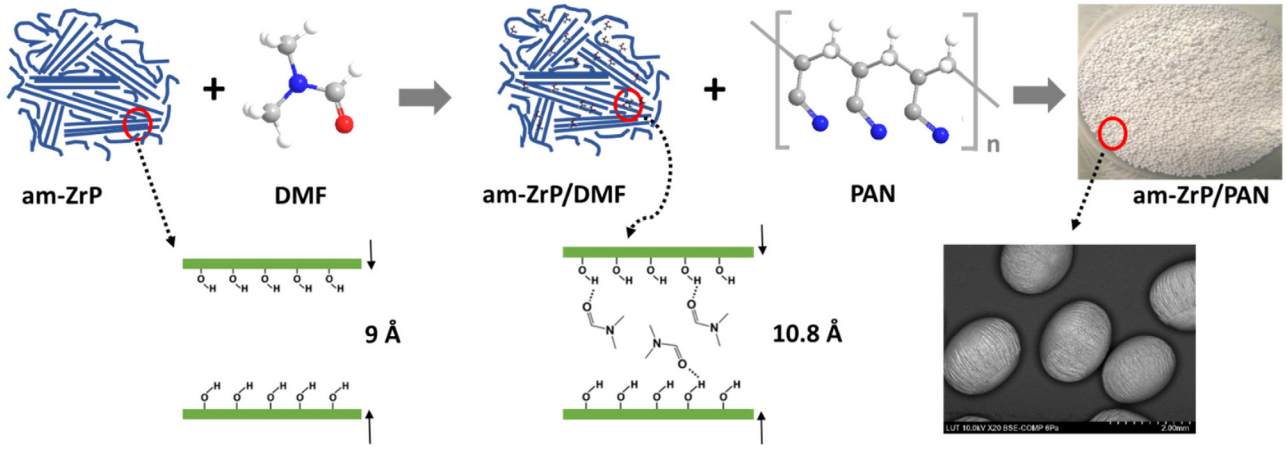

Scheme 1. Schematic presentation of the synthesis of am-ZrP/DMF/PAN (am-ZrP/PAN).

intraparticle diffusion model based on Fick's law, Eq. (5), where D_j is the intraparticle diffusion coefficient of species j, $\hat{q}_j$ is local concentration and r is the radial coordinate and r_p is the particle radius.

$$\frac{\partial \hat{q}_j}{\partial t} = \frac{1}{r^2}\frac{\partial}{\partial r}\left(r^2 D_j \frac{\partial \hat{q}_j}{\partial r}\right), \left.\frac{\partial \hat{q}_j}{\partial r}\right|_{r=0} = 0, \hat{q}_j|_{r=r_p} = f(c_j) \quad (5)$$

The second order PDE system was discretized in the radial direction of the particle using a finite difference scheme and the resulting ODE system was solved numerically using the method of lines [38]. The temporal derivatives are

$$0 < r < r_p: \quad \frac{d\hat{q}_j}{dt} = D_j\left(\frac{2}{r}\frac{d\hat{q}_j}{dr} + \frac{d^2\hat{q}_j}{dr^2}\right)$$
$$r = 0: \quad \frac{d\hat{q}_j}{dt} = 3D_j\frac{d^2\hat{q}_j}{dr^2}$$
$$r = r_p: \quad \frac{d\hat{q}_j}{dt} = 0 \quad (6)$$

The change in liquid phase concentration was calculated from the mass balance assuming that all mass transfer resistance is within the particles (that are relatively large here)

$$\frac{dc_j^L}{dt} = -\frac{A_{tot}}{V^L}D_j\left.\frac{d\hat{q}_j}{dr}\right|_{r=r_p} \quad (7)$$

where A_{tot} is the total surface area of the particles (assumed to be monodisperse and spherical) and V^L is the volume of the bulk liquid phase. The first and second order derivatives in Eq. (6) were calculated in a stepwise manner. Three-point centered approximation was used to calculate the first derivative $d\hat{q}/dr$. The second derivative was obtained by applying the same centered approximation for the first derivative thus obtained.

As seen in Eq. (5), the am-ZrP/PAN material was treated as a homogeneous medium as the inorganic particles were assumed to be dispersed homogeneously in the polymer matrix. For Co, a value of $D_{Co} = 4.31{\cdot}10^{-12}\,m^2/s$ was obtained ($R^2 = 0.990$). The values obtained for Dy and Nd were an order of magnitude lower ($D_{Dy} = 1.05{\cdot}10^{-13}\,m^2/s$, $R^2 = 0.937$; $D_{Nd} = 1.02{\cdot}10^{-13}\,m^2/s$, $R^2 = 0.967$). Slower diffusion of Dy and Nd compared to Co is understandable considering their larger hydrated radii [39,40]. The results show that a simple diffusion model is sufficient for a quantitative description of diffusion in an am-ZrP/PAN composite. However, the data available is not sufficient to distinguish between diffusion resistance in the polymer phase and in the am-ZrP particles.

Table 3
Interpretation of the intercalation compounds of α-ZrP/DMF, α-SnP/DMF and am-ZrP/DMF.

Inorganic material	basal spacing (Å)	Intercalated basal spacing (Å)	Diameter of DMF (Å)	Diameter of H_2O molecular (Å)	References
α-SnP	7.8	13.3	3.5	2.8	[26]
α-ZrP	7.6	11.2	3.5	2.8	[27]
am-ZrP	9.0[a]	10.8	3.5	2.8	this work

[a] The layer space of semicrystalline am-ZrP material.

3.7. Effect of pH on adsorption

Investigations of the effect of solution pH on Co, Nd and Dy adsorption were conducted in 1-mM ternary solutions in a pH range from 1 to 6. Speciation calculations (Minteq) did not show any precipitation of metals in that range. The uptake of Nd and Dy (Fig. 6) increased rather sharply with increasing pH and reached a plateau at approximately pH 2.5. In contrast, the Co uptake gradient was considerably lower and the uptake of Co was very low (< 0.05 meq/g) below pH 2.6,

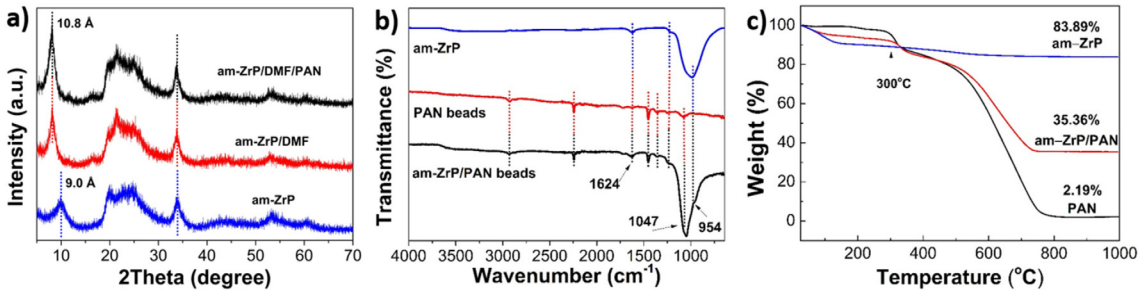

Fig. 3. a) XRD pattern of the synthesized am-ZrP, am-ZrP/DMF and am-ZrP/PAN. b) FTIR spectra of the am-ZrP, PAN beads and am-ZrP/PAN beads. c) TGA curves of the PAN beads, am-ZrP and am-ZrP/PAN beads.

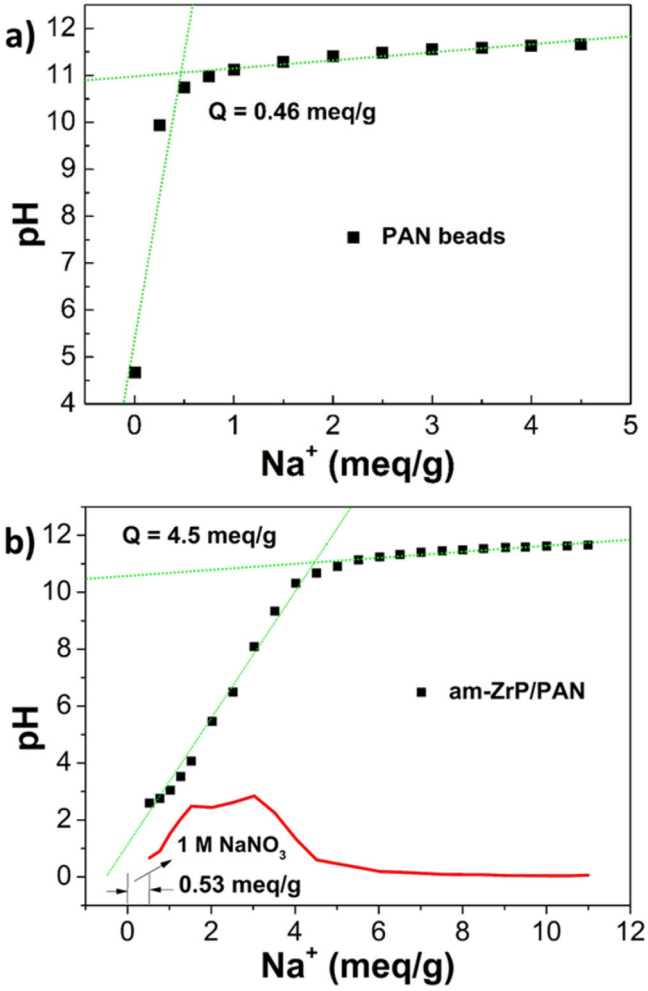

Fig. 4. Titration curves of a) pure PAN beads and b) am-ZrP/PAN beads in 1 M $NaNO_3$. The red colour curve in panel b represents the first derivative of the am-ZrP/PAN beads titration curve.

reaching its maximum of 0.26 meq/g at pH 6. The uptake of Co increased after pH 4.3, causing the slight uptake decrease of Nd and Dy. Maximum uptake values of Co, Dy and Nd were determined at pH 6.0 as 0.26, 0.59, and 0.58 meq/g, respectively, totalling 1.42 meq/g. However, the strong sorption of Co decreased the sorption of Nd and Dy and increased the difficulty of separation. Thus, the subsequent experiments

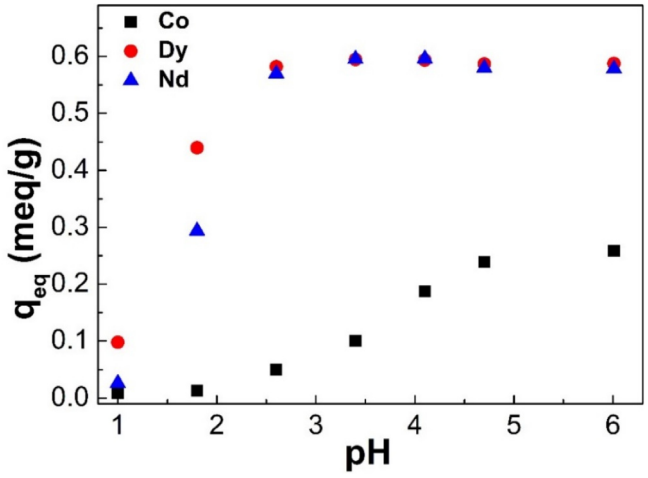

Fig. 6. Metal-uptake curves of the effect of pH on the sorption of Co, Nd and Dy with the initial concentration of 1 mM by am-ZrP/PAN composite.

were done at lower pH condition at pH 1.8 where low Co uptake and high separation factors.

3.8. Proposed mechanism for the enhanced adsorption of am-ZrP/PAN

Metal uptake of am-ZrP increased about 50% from 1.65 to 2.43 meq/g on fabrication of am-ZrP/PAN beads (calculated to inorganic counterpart) [16]. The increased uptake is assumed to result from DMF intercalation into the interlayer of ZrP. The interlayer spacing of the pure am-ZrP (semicrystalline) can be considered as partially inaccessible for the rather large hydrated metal ions; at a minimum, the diffusional resistance can be considered high [41]. After DMF intercalation and expansion of the interlayer distance from 9 to 10.8 Å, the metal-ion diffusion to the ion-exchange sites located at the interlayer is considered easier and thereby improves the metal uptake properties of the materials.

3.9. Fixed-bed column study

3.9.1. Separation Co, Nd and Dy from a dilute solution

Recovery and removal of Co from a dilute solution (1 mM equimolar Co, Nd and Dy) at pH 1.8 was very efficient using the am-ZrP/PAN composite material in an adsorption column (Fig. 7a). The breakthrough curves of Co, Nd and Dy during loading are consistent with the adsorption equilibrium data in the batch experiment (Fig. 6); the metals were preferred in the following order: Dy > Nd > Co. Thereafter, a

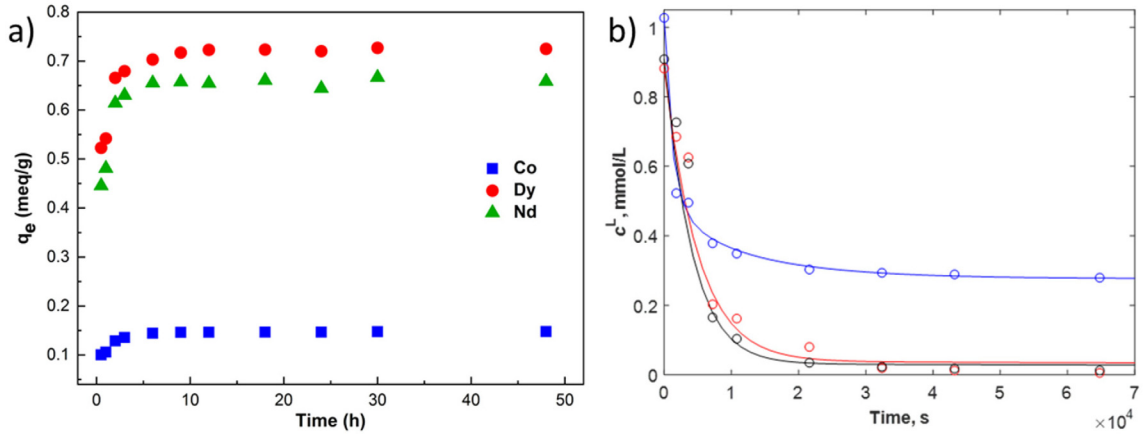

Fig. 5. a) The effect of contact time on the adsorption kinetics of 1 mM Co, Nd and Dy nitrite solution into amorphous ZrP at 23 °C and pH 3; b) The sorption kinetics fitting curves of Co (blue), Nd (black) and Dy (red) into am-ZrP/PAN composite at 23 °C and pH 3.

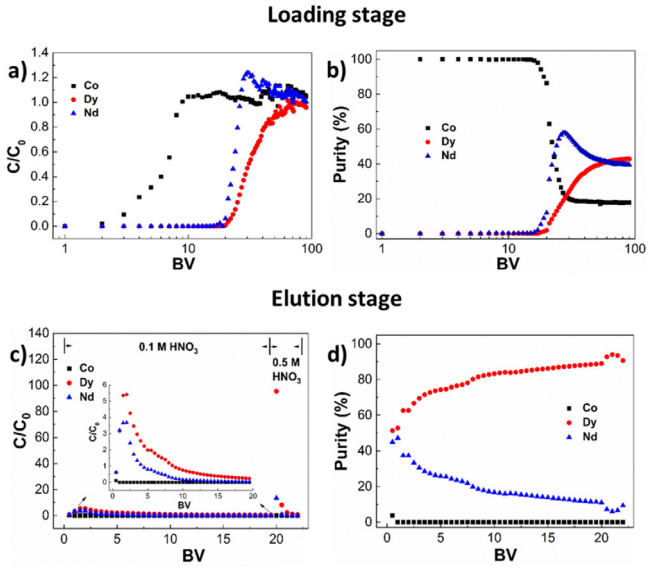

Fig. 7. a) Breakthrough curves of Co, Nd and Dy with initial concentrations of 1 mmol/L in HNO_3 (pH 1.8). b) Purity of Co, Nd and Dy in the effluent at loading phase. c) Elution curves of Co, Nd and Dy. d) Purity of Co, Nd and Dy in the effluent at elution phase.

slightly higher concentration of Co than in the feed between 8 and 20 BV was observed, perhaps due to displacement from the ion-exchange sites by Nd and Dy (which have higher valence). The purity of Co in the effluent (Fig. 7b) was 98.7% during the first 20 BV. Competitive sorption also explains the overshoot in Nd concentration (maximum $C/C^0 = 1.2$ for Nd), as Dy had the strongest affinity to the composite material (K_d(Co) = 6, K_d(Nd) = 180 and K_d(Dy) = 458 at pH 1.8). Separation of Nd and Dy was not very good partially because of strong mass transfer resistance (see Section 3.6). The purity of Nd at the column outlet reached a value of only 0.6.

After 91 BV of feed, the column was almost fully loaded and the metal amounts in the column were calculated as 0.03 meq/g of Co, 0.78 meq/g of Dy and 0.38 meq/g of Nd. The column bed was washed with dilute acid at pH 1.8 and elution of the metals was performed in two steps (0.1 M HNO_3 followed by 0.5 HNO_3) (Fig. 7c). Co was already eluted very effectively during washing and was not detected in the effluent after the first 1 BV. The purity of Dy in the effluent was higher than 80% between 7 and 20 BVs (Fig. 7d) and purity during the whole elution (0–24 BV) was 67%.

3.9.2. Separation of Co, Nd and Dy from a concentrated solution

To study the separation under more practical conditions (i.e., higher concentrations), a mixture with a total concentration of 1.2 g/L (approximately 10.7% of Co, 41.1% of Nd and 48.2% of Dy) was used as the feed. Loading the column until saturation is not useful as there is very little separation between Nd and Dy from 30 to 90 BV (Fig. 7). Therefore, the column was loaded only to approximately 10% relative to the maximum loading. Typically, the metal feed solution was at pH 1.8 while the elution was performed with 0.2 M HNO_3. The effects of temperature, flow rate and acid concentration of the eluent on the metal separation were studied.

Nd and Dy breakthrough occurred at approximately 1 BV when the total concentration of metals in the feed solution was 1.2 g/L (Fig. 8a). This is very early compared to the dilute solution in Fig. 7, where the breakthrough occurred at approximately 20 BV. The sharpness of the Co profile compared to Nd and Dy profiles is due to its higher diffusion coefficient and thermodynamic effects (less steep isotherm).

Increasing the temperature from 23 to 50 °C improved the separation of Co from Nd and Dy. This is because mass transfer is slow at 23 °C (see Section 3.6) but increases with temperature as seen as the steeper rear part of the Co elution profile (Fig. 8a and 8b). Increasing the temperature to 50 °C and decreasing the flow rate from 1 BV/h to 0.5 BV/h (Fig. 8a and c) gave a significantly better separation and Co could be recovered with high yield and purity. Separation between Nd and Dy was not very good as they were eluted almost identically when using 0.2 M HNO_3 as eluent. Increasing the HNO_3 concentration of the eluent to 0.5 M (Fig. 8d) did not improve the metal separation but shorted the process cycle.

It can be concluded that low acid concentration in the eluent is beneficial for metal separation but high concentration is beneficial for productivity. Similar to previous studies [16,42], a multistep gradient elution process where the composition of the mobile phase was changed stepwise was studied [42]. Here, 0.1, 0.2, 0.5 and 1 M HNO_3 were sequentially used in the elution at 50 °C. The separation of Co from Nd and Dy was significantly enhanced with the gradient elution (Fig. 8e and f).

The local purity of the effluent (in wt%) with respect to each metal is shown in Fig. 8f. In practice, the effluent should be fractionated into three product fractions such that each metal is recovered with sufficient yield and purity. Collecting the first 1.43 BV of the effluent to the first product fraction results in a recovery yield of 90% and (volume-average) purity of 91 wt% for Co. Higher purity can be achieved at the cost of decreasing yield; for example, with 95 wt% purity the yield of Co is 86%. The recovery of Co is quite efficient considering that its content in the feed is only 10 wt%. Dy can be collected as the last product fraction. For example, starting the collection at 3.2 BV results in 80 wt% purity and 55% recovery yield for Dy. Between these two fractions, Nd is recovered with 58 wt% purity and 82% yield.

3.9.3. Separation of Co, Nd and Dy from a simulated magnet leachate

To study the suitability of the am-ZrP/PAN beads in a practical setting of metal separation, a simulated magnet leachate was used as feed solution. The feed (7.6 g/L total) contained 1.4% of Co, 9.3% of Dy and 89.3% of Nd. Recovery of all metals from such a ternary solution is extremely difficult as the major component, Nd, is eluted in the middle between Co and Dy. The gradient elution method was chosen based on the developed process on varying conditions of the column study, using 1.2 g/L solution.

From the effluent concentration profiles in Fig. 9a, it was possible to recover some Co at high purity even though its concentration in the feed was only 1.4%. On the other hand, some Dy was recovered at the later of the fractions where the column is being fully regenerated with 1 M HNO_3. To better visualize the trade-off between purity and yield, the curves in Fig. 9b show the Pareto frontiers for each metal. The vertical dashed lines indicate the feed composition. The further the curve is to the right, the higher the increase in purity during the gradient elution. In these calculations, it is assumed that a recycle fraction is collected during 4.1–4.7 BV of elution, as at this interval the Nd/Dy ratio is almost the same as in the feed and no separation is achieved. For each of the three metals, the Pareto frontiers show that it is possible to obtain fractions with significantly improved purity relative to the feed.

3.10. Column regeneration

Efficient regeneration of ion-exchange materials is essential considering the economic usability of the materials. The XRD of am-ZrP/PAN was measured after the third and tenth column run. The XRD pattern of the used am-ZrP/PAN beads (Fig. 10) showed clear shifts after regeneration cycles. The interlayer space of am-ZrP after Run 3 and Run 10 showed a decrease of 1.0 Å and 1.4 Å, respectively, compared to that of unused am-ZrP. The results suggest that DMF was released from the layers during the ion-exchange cycle. The XRD results revealed the possibility for gradual shrinkage of interlayer space of am-ZrP (semicrystalline) from 10.8 Å back to 9.4 Å.

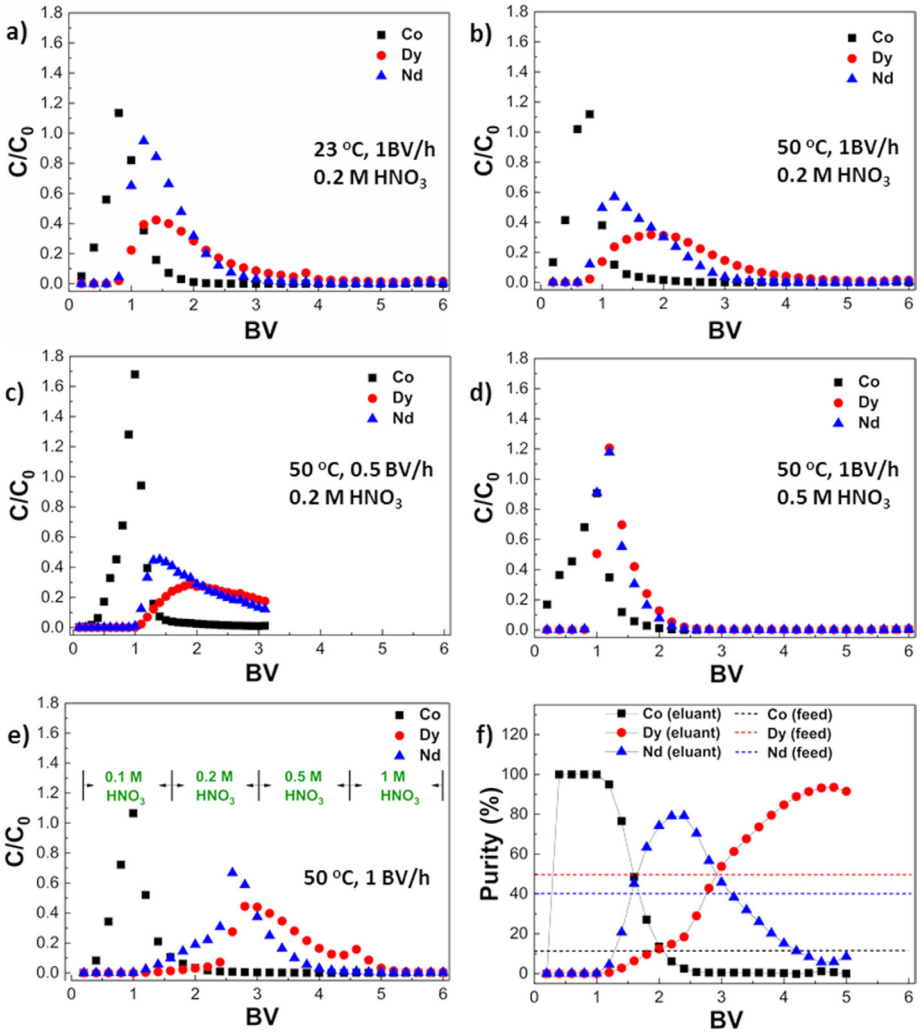

Fig. 8. Elution curves of Co, Nd and Dy from an approximately 10% loaded column using the 1.2 g/L feed (approximately 10.7% of Co, 41.1% of Nd and 48.2% of Dy). a) 0.2 M HNO_3, 23 °C and 1 BV/h; b) 0.2 M HNO_3, 50 °C and 1 BV/h; c) 0.2 M HNO_3, 50 °C and 0.5 BV/h; d) 0.5 M HNO_3, 50 °C and 0.5 BV/h. e) Gradient elution, 1 BV/h at 50 °C. f) Purity of Co, Nd and Dy in eluent corresponding to the gradient elution in figure e.

4. Conclusions

We synthesized an am-ZrP/PAN composite in bead form to solve possible pressure build-up problems in scale-up column separation. Am-ZrP was evenly distributed in the am-ZrP/PAN composite beads. An interesting discovery was that DMF expanded interlayers of am-ZrP, which improved the efficiency of metal uptake. In addition, we demonstrated an efficient gradient elution process from the perspective of chemical engineering. In column separation experiments effects of feed concentrations, loading degree, temperature, flowrates, and concentration of the HNO_3 eluent were studied. As a result, feasible operating conditions to perform the separation were suggested. The purity of simulated leachate was enhanced to 87.9% of Co, 96.4% of Nd and 40% of Dy in different stage effluent using a single column. The results were promising and

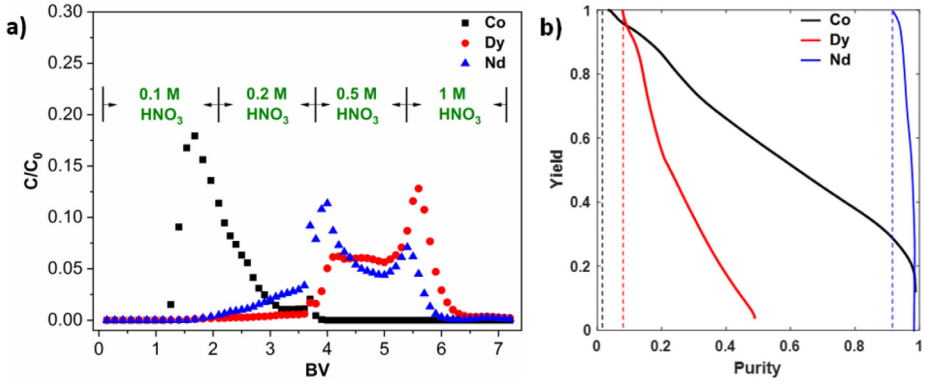

Fig. 9. Separation from a synthetic magnet leachate. a) Gradient elution curves of Co, Nd and Dy (approximately 10% loaded column) with a running speed of 1 BV/h at 50 °C. b) Relationship between the purity and yield during gradient elution.

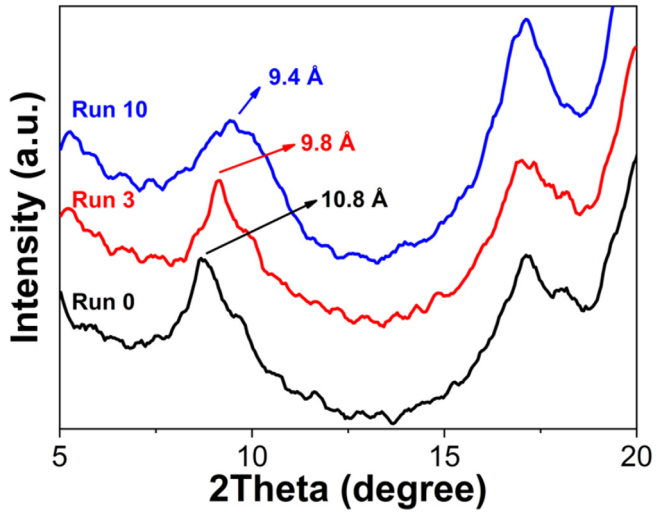

Fig. 10. XRD pattern of used am-ZrP/PAN beads after Run 0, Run 3 and Run 10 of the column study.

meaningful for further purification using a continuous simulated moving bed. Although the DMF was gradually released in the column regeneration study, the enhanced uptake results provide a promising direction for future study on intercalation chemistry.

Acknowledgments

The research leading to these results received funding from the European Community's Seventh Framework Programme ([FP7/2007-2013]) under grant agreement no. 607411 (MC-ITN EREAN: European Rare Earth Magnet Recycling Network, http://www.erean.eu). This publication reflects only the authors' views, exempting the Community from any liability. Financial support from Academy of Finland through the RAMI infrastructure project (293109) is acknowledged for the X-ray tomography results. The authors would like to thank Dr. Toni Väkiparta for his contribution to the measurement and comments on the size distribution of am-ZrP/PAN. The authors would like to dedicate this work to the memory of our beloved Prof. Risto Harjula for his kind teaching, supervision and friendship.

References

[1] K. Binnemans, P.T. Jones, B. Blanpain, T. Van Gerven, Y. Yang, A. Walton, M. Buchert, Recycling of rare earths: a critical review, J. Clean. Prod. 51 (2013) 1–22.
[2] Y. Yang, A. Walton, R. Sheridan, K. Güth, R. Gauß, O. Gutfleisch, M. Buchert, B.-M. Steenari, T. Van Gerven, P.T. Jones, REE recovery from end-of-life NdFeB permanent magnet scrap: a critical review, J. Sustain. Metal. 3 (2017) 122–149.
[3] P. Froehlich, T. Lorenz, G. Martin, B. Brett, M. Bertau, Valuable metals—recovery processes, current trends, and recycling strategies, Angew. Chem. Int. Ed. 56 (2017) 2544–2580.
[4] A. El-Moneim, A. Gebert, M. Uhlemann, O. Gutfleisch, L. Schultz, The influence of Co and Ga additions on the corrosion behavior of nanocrystalline NdFeB magnets, Corrosion Sci. 44 (2002) 1857–1874.
[5] E. Alonso, A.M. Sherman, T.J. Wallington, M.P. Everson, F.R. Field, R. Roth, R.E. Kirchain, Evaluating rare earth element availability: a case with revolutionary demand from clean technologies, Environ. Sci. Technol. 46 (2012) 3406–3414.
[6] European Commission, Report on the critical raw materials for the EU, 2017, pp. 1–8.
[7] K. Binnemans, P.T. Jones, T. Müller, L. Yurramendi, Rare earths and the balance problem: how to deal with changing markets? J. Sustain. Metal. (2018) 1–21.
[8] P. Venkatesan, T. Vander Hoogerstraete, T. Hennebel, K. Binnemans, J. Sietsma, Y. Yang, Selective electrochemical extraction of REEs from NdFeB magnet waste at room temperature, Green Chem. 20 (2018) 1065–1073.
[9] M.K. Jha, A. Kumari, R. Panda, J.R. Kumar, K. Yoo, J.Y. Lee, Review on hydrometallurgical recovery of rare earth metals, Hydrometallurgy 165 (2016) 2–26.
[10] P.J. Panak, A. Geist, Complexation and extraction of trivalent actinides and lanthanides by triazinylpyridine N-donor ligands, Chem. Rev. 113 (2013) 1199–1236.
[11] X.-Z. Li, L.-P. Zhou, L.-L. Yan, Y.-M. Dong, Z.-L. Bai, X.-Q. Sun, J. Diwu, S. Wang, J.-C. Bünzli, Q.-F. Sun, A supramolecular lanthanide separation approach based on multivalent cooperative enhancement of metal ion selectivity, Nat. Commun. 9 (2018) 547.
[12] L.M. Inamuddin, M. Luqman, Ion exchange technology I: theory and materials, Springer 10 (2012) 978–994.
[13] F. Xie, T.A. Zhang, D. Dreisinger, F. Doyle, A critical review on solvent extraction of rare earths from aqueous solutions, Miner. Eng. 56 (2014) 10–28.
[14] A. Clearfield, Inorganic ion exchangers, past, present, and future, Solvent Extract. Ion Exchange 18 (2000) 655–678.
[15] J. Xu, E. Wiikinkoski, R. Koivula, W. Zhang, B. Ebin, R. Harjula, HF-free synthesis of α-zirconium phosphate and its use as ion exchanger for separation of Nd (III) and Dy (III) from a ternary Co–Nd–Dy system, J. Sustain. Metal. 3 (2017) 646–658.
[16] J. Xu, R. Koivula, W. Zhang, E. Wiikinkoski, S. Hietala, R. Harjula, Separation of cobalt, neodymium and dysprosium using amorphous zirconium phosphate, Hydrometallurgy 175 (2018) 170–178.
[17] S. İnan, R. Koivula, R. Harjula, Removal of 63Ni and 57Co from aqueous solution using antimony doped tin dioxide–polyacrylonitrile (Sb doped SnO2–PAN) composite ion-exchangers, J. Radioanal. Nucl. Chem. 299 (2014) 901–908.
[18] Q. Zhang, Q. Du, T. Jiao, Z. Zhang, S. Wang, Q. Sun, F. Gao, Rationally designed porous polystyrene encapsulated zirconium phosphate nanocomposite for highly efficient fluoride uptake in waters, Sci. Rep. 3 (2013).
[19] H.C. Wang, S.Y. Lin, A.C. Tang, B.P. Singh, H.C. Tong, C.Y. Chen, Y.C. Lee, T.L. Tsai, R.S. Liu, Mesoporous silica particles integrated with all-inorganic CsPbBr 3 perovskite quantum-dot nanocomposites (MP-PQDs) with high stability and wide color gamut used for backlight display, Angew. Chem. Int. Ed. 55 (2016) 7924–7929.
[20] C. Dwivedi, A. Kumar, K.K. Singh, A.K. Juby, M. Kumar, P.K. Wattal, P.N. Bajaj, Copper hexacyanoferrate–polymer composite beads for cesium ion removal: synthesis, characterization, sorption, and kinetic studies, J. Appl. Polym. Sci. 129 (2013) 152–160.
[21] Z. Geng, Y. Lin, X. Yu, Q. Shen, L. Ma, Z. Li, N. Pan, X. Wang, Highly efficient dye adsorption and removal: a functional hybrid of reduced graphene oxide–Fe 3 O 4 nanoparticles as an easily regenerative adsorbent, J. Mater. Chem. 22 (2012) 3527–3535.
[22] J.-K. Moon, K.-W. Kim, C.-H. Jung, Y.-G. Shul, E.-H. Lee, Preparation of organic-inorganic composite adsorbent beads for removal of radionuclides and heavy metal ions, J. Radioanal. Nucl. Chem. 246 (2000) 299–307.
[23] J.-K. Moon, C.-H. Jung, E.-H. Lee, H.-T. Kim, Y.-G. Shul, Preparation of PAN-zeolite 4A composite ion exchanger and its uptake behavior for Sr and Cs ions in acid solution, Korean J. Chem. Eng. 19 (2002) 838–842.
[24] S. İnan, Y. Altaş, Preparation of zirconium–manganese oxide/polyacrylonitrile (Zr–Mn oxide/PAN) composite spheres and the investigation of Sr (II) sorption by experimental design, Chem. Eng. J. 168 (2011) 1263–1271.
[25] N. Mann, T. Todd, T. Tranter, F. Šebesta, Development of novel composite sorbents for the removal of actinides from environmental and analytical solutions, J. Radioanal. Nucl. Chem. 254 (2002) 41–45.
[26] G. Naidu, P. Loganathan, S. Jeong, M.A.H. Johir, V.H.P. To, J. Kandasamy, S. Vigneswaran, Rubidium extraction using an organic polymer encapsulated potassium copper hexacyanoferrate sorbent, Chem. Eng. J. 306 (2016) 31–42.
[27] S. Riaño, K. Binnemans, Extraction and separation of neodymium and dysprosium from used NdFeB magnets: an application of ionic liquids in solvent extraction towards the recycling of magnets, Green Chem. 17 (2015) 2931–2942.
[28] T. Vander Hoogerstraete, B. Blanpain, T. Van Gerven, K. Binnemans, From NdFeB magnets towards the rare-earth oxides: a recycling process consuming only oxalic acid, RSC Adv. 4 (2014) 64099–64111.
[29] C. Trobajo, S.A. Khainakov, A. Espina, J.R. García, On the synthesis of α-zirconium phosphate, Chem. Mater. 12 (2000) 1787–1790.
[30] E. Rodriguez-Castellon, A. Rodriguez-Garcia, S. Bruque, Intercalation of polar organic compounds into tin (IV) hydrogenphosphate monohydrate, Inorg. Chem. 24 (1985) 1187–1190.
[31] D. Behrendt, K. Beneke, G. Lagaly, Intercalation compounds of zirconium phosphate, Angew. Chem. Int. Ed. 15 (1976) 544–545.
[32] A. Clearfield, R.M. Tindwa, On the mechanism of ion exchange in zirconium phosphates—XXI intercalation of amines by α-zirconium phosphate, J. Inorg. Nucl. Chem. 41 (1979) 871–878.
[33] S. Horsley, D. Nowell, D. Stewart, The infrared and Raman spectra of α-zirconium phosphate, Spectrochim. Acta. A: Mol. Spectrosc. 30 (1974) 535–541.
[34] A. Tarafdar, A. Panda, N. Pradhan, P. Pramanik, Synthesis of spherical mesostructured zirconium phosphate with acidic properties, Micropor. Mesopor. Mater. 95 (2006) 360–365.
[35] Z. Wang, Y. Feng, X. Hao, W. Huang, X. Feng, A novel potential-responsive ion exchange film system for heavy metal removal, J. Mater. Chem. A 2 (2014) 10263–10272.
[36] F. Ma, W. Shi, H. Meng, Z. Li, W. Zhou, L. Zhang, Preparation, characterization and ion-exchange behavior of polyantimonic acid-polyacrylonitrile (PAA–PAN) composite beads for strontium (II), J. Radioanal. Nucl. Chem. 308 (2016) 155–163.
[37] F. Helfferich, Ion Exchange, Dover, New York, 1995.
[38] W. Schiesser, The Numerical Methods of Lines, Integration of Partial Differential Equations, Academic Press, San Diego, 1991.
[39] E. Nightingale Jr, Phenomenological theory of ion solvation. Effective radii of hydrated ions, J. Phys. Chem. 63 (1959) 1381–1387.
[40] R. Lundqvist, E. Hulet, P. Baisden, Electromigration method in tracer studies of complex chemistry, Acta Chem. Scand. Ser. A 35 (1981) 653–661.
[41] J. García-Glez, C. Trobajo, S.A. Khainakov, Z. Amghouz, α-Titanium phosphate intercalated with propylamine: an alternative pathway for efficient europium (III) uptake into layered tetravalent metal phosphates, Arab. J. Chem. 10 (2017) 885–894.
[42] P. Jandera, J. Churacek, Gradient Elution in Column Liquid Chromatography: Theory and Practice, Elsevier, 1985.